Reduced-gradient analysis of molecular adsorption on graphene with nonlocal density functionals

T. Jenkins,[1,2] D. Chakraborty,[1,2] K. Berland,[3,*] and T. Thonhauser[1,2,†]

[1]*Department of Physics, Wake Forest University, Winston-Salem, North Carolina 27109, USA*

[2]*Center for Functional Materials, Wake Forest University, Winston-Salem, North Carolina 27109, USA*

[3]*Faculty of Science and Technology, Norwegian University of Life Sciences, Norway*

(Received 3 November 2023; revised 21 December 2023; accepted 2 January 2024; published 19 January 2024)

Graphene has garnered tremendous interest in the last decade due to its great potential for applications in almost every scientific and engineering discipline. The adsorption of molecules onto graphene is itself also of significant interest, including in catalysis and trace molecule detection. However, density functional theory has traditionally struggled to accurately model surface adsorption involving long-range dispersion interactions between a molecule and a substrate, accentuating the need for comprehensive benchmarking and analysis. Here, we test the accuracy of several functionals in describing the adsorption energy of graphene–molecule adsorption complexes, including several van der Waals density functionals as well as the nonlocal correlation functional rVV10 and the dispersion-corrected PBE-D3. We find that the highest accuracy is provided by vdW–DF2 and the two realizations of vdW–DF3, the most recent generations of the van der Waals density functional family. In addition, we use a reduced-gradient analysis technique to examine the material's exchange energy. This analysis resolves contributions to the exchange interaction energy as a function of the reduced-gradient s, revealing regimes of s that are important components of the interaction energy of these systems. In doing so, we identify the best functionals currently available and initiate discussion on desirable traits of each functional for modeling surface adsorption.

DOI: 10.1103/PhysRevB.109.035427

I. INTRODUCTION

Molecular surface adsorption has seen wide use and great impact on technology and industry, the properties of which vary greatly depending on the molecule or substrate used. Graphene in particular is a material that has experienced a rapid growth in interest—as an adsorption substrate it has been studied in many different contexts, including catalysis [1–3], lubrication [4–6], corrosion [7], modeling astrophysical conditions [8], and many more [9–12]. Advancements have also been made towards water filtration [13–15], DNA sequencing [16–18], and trace molecule detection with methods such as surface-enhanced Raman spectroscopy, for which graphene was found to act as an excellent nanoplatform due to its stability and uniform structure [19].

The inclusion of dispersion forces, vital for accurately modeling surface adsorption, has been one of the most important advances in the development of density functional theory (DFT) in the last two decades [20–25]. Such dispersion forces are missing in widely used generalized gradient approximation (GGA) [26–31], and one approach to include them is through the use of a correction to an already existing functional, as is done with the DFT-D methods [26,32–34]. Another method to treat these cases is with a meta-generalized gradient approximation (meta-GGA) functional. First created by Tao and Perdew in the form of the Tao-Perdew-Staroverov-Scuseria functional (TPSS), derivatives such as M06L and SCAN better account for dispersion-bonded systems [35–38]. One can also use an explicit nonlocal correlation term that accounts for long-range dispersion interactions as a functional of the electron density alone. Langreth, Lundqvist, and coworkers developed the first of these so-called van der Waals density functionals (vdW–DF), a family that has grown significantly since its inception [27,39–49]. The vdW–DF functional introduced nonlocal correlation as a separate term containing a density-density interaction kernel that was inspired by the plasmon-pole model and adheres to four exact physical constraints. It also retains a gradient-corrected exchange at the GGA-level of theory, which is based on the local electronic density $n(\mathbf{r})$ and the reduced-gradient, $s(\mathbf{r}) \propto |\nabla n(\mathbf{r})|/n(\mathbf{r})^{4/3}$, and is vital to the short- and mid-range regions of binding curves; in fact, using an exchange description at the local density approximation (LDA) level, using only $n(\mathbf{r})$, causes significant spurious binding [50,51].

The potential applications of these functionals towards graphene adsorption were recognized soon after the development of vdW–DF, and were the subject of extensive research by Schröder and coworkers: early examples included studies of vdW–DF on the adsorption of aromatic organic molecules and later branched out into more varied and complex systems [52–59]. The variety of adsorbates studied over the last two decades, combined with the growing presence of new and improved nonlocal density functionals, makes clear the need for a comprehensive benchmark review of graphene adsorption. In this study, we apply nine such functionals to a dataset of 21 different molecules adsorbed onto graphene. These 21

*kristian.berland@nmbu.no

†thonhauser@wfu.edu

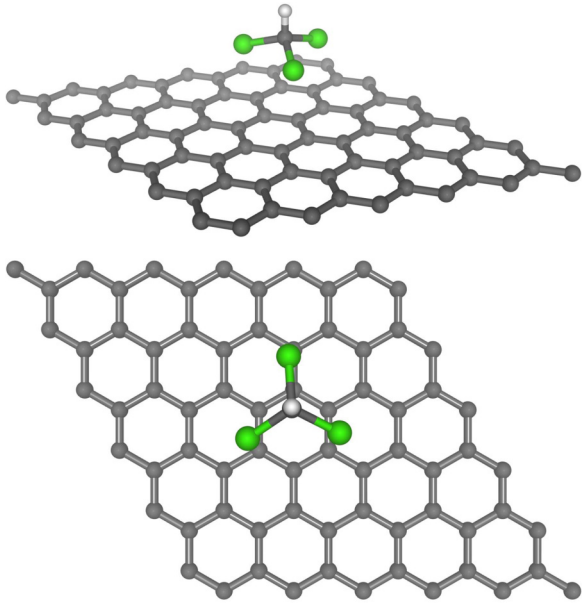

FIG. 1. Side and top view of chloroform ($CHCl_3$) adsorbed onto a graphene. H is in white, Cl in green, and C in black.

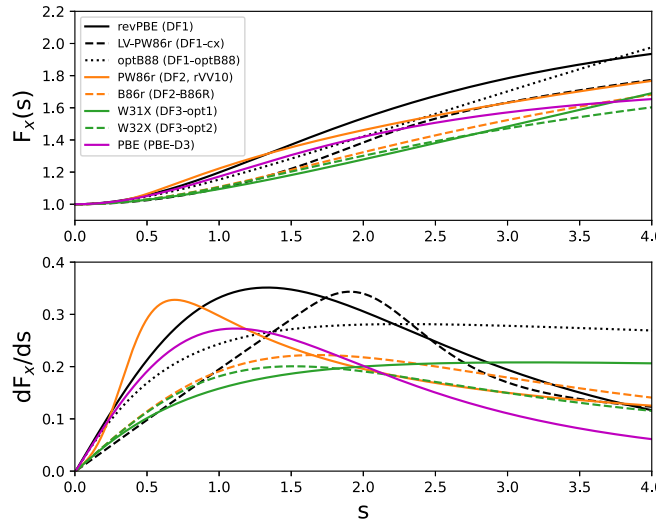

FIG. 2. Exchange enhancement factors and their derivatives for the eight functionals included in our study. The rVV10 enhancement factor is the same as that of DF2, i.e., revised PW86 exchange [50].

systems are subdivided into six classes consisting of noble gases [60], chloroform (as shown in Fig. 1) [61], diatomic molecules [60], *n*-alkanes of the form C_nH_{2n+2} [62], aromatic hydrocarbons [63], and nucleobases [64]. All reference energies, save for the nucleobases and chloroform, stem from temperature-programmed desorption (TPD) [65]. Nucleobase adsorption energies were instead obtained via isothermal titration calorimetry (ITC) [66], while the chloroform adsorption energy comes from single-atom gas chromatography [67].

While dispersion interactions have an important role in physisorption, they vary far more slowly with separation than the exchange effects, which are related to orbital overlaps [50,51,68]. Crafting appropriate GGA-exchange-enhancement factors $F_x(s)$ has thus been an important part of vdW–DF development and is related to the GGA exchange energy by

$$E_x^{GGA}[n] = \int d^3\mathbf{r} n(\mathbf{r}) \epsilon_x^{LDA}(n(\mathbf{r})) F_x(s), \tag{1}$$

where $\epsilon_x^{LDA}(n(\mathbf{r}))$ is the exchange energy per particle at the LDA level of theory. Various exchange-enhancement factors are shown in Fig. 2. To analyze trends arising from the exchange choice, we resolve the exchange energy in s as follows:

$$e_{gx}(s) = -\frac{3}{4}\left(\frac{3}{\pi}\right)^{1/3} \int d^3\mathbf{r} n^{4/3}[F_x(s(\mathbf{r})) - 1]\delta(s - s(\mathbf{r})), \tag{2}$$

similar to the reduced-gradient analysis in Refs. [50,68,69]. Moreover, we recently applied this analysis to a range of material classes, explaining why good functional performance for one class of systems in no way guarantees strong performance for other classes of systems [68]. Thus, using reduced-gradient analysis can highlight a means to improve graphene adsorption modeling in future functional development.

II. COMPUTATIONAL DETAILS

All calculations were done using the QUANTUM ESPRESSO (QE) package [70] and PBE ultrasoft pseudopotentials of Garrity, Bennett, Rabe, and Vanderbilt (GBRV) [71], with a wave-function cutoff of 50 Rydberg and a density cutoff of 600 Rydberg.

Optimized lattice parameters of graphene were first calculated for each functional. These calculations were performed with a spacing of 20 Å between individual layers of graphene, and a $12 \times 12 \times 1$ k-point mesh in the sampling of the Brillouin zone. Optimizations of the adsorption system and its separate constituents used Γ-point sampling of the Brillouin zone and convergence criteria of 1×10^{-8} Rydberg for energies and 1×10^{-4} Rydberg/Bohr for forces. For each adsorbate, $n \times n \times 1$ supercells of graphene were chosen to provide a minimum 8.0 Å cushion between molecules in adjacent cells.

For nucleobases, Ref. [64] provides experimental adsorption results in an alkaline environment and reports separately the solvation energies for each nucleobase. Following the definition of the solvation energy outlined in Refs. [64] and [72], we take the reported experimental adsorption energy minus the solvation energy as the reference value in these calculations. Out of the four nucleobases, we found unusually large errors in the adsorption energy for thymine relative to experiment. We believe that this could be due to a possible error in the experimental measurements, as other DFT studies show similar disagreement for thymine [73,74]. For this reason, we have chosen to omit thymine from the results shown here. Results including the thymine-graphene system are given in the Supplemental Material [75].

In the reduced-gradient analysis, we compute the change arising due to adsorption by

$$\Delta e_{gx}(s) = e_{gx}^{system}(s) - e_{gx}^{molecule}(s) - e_{gx}^{graphene}(s). \tag{3}$$

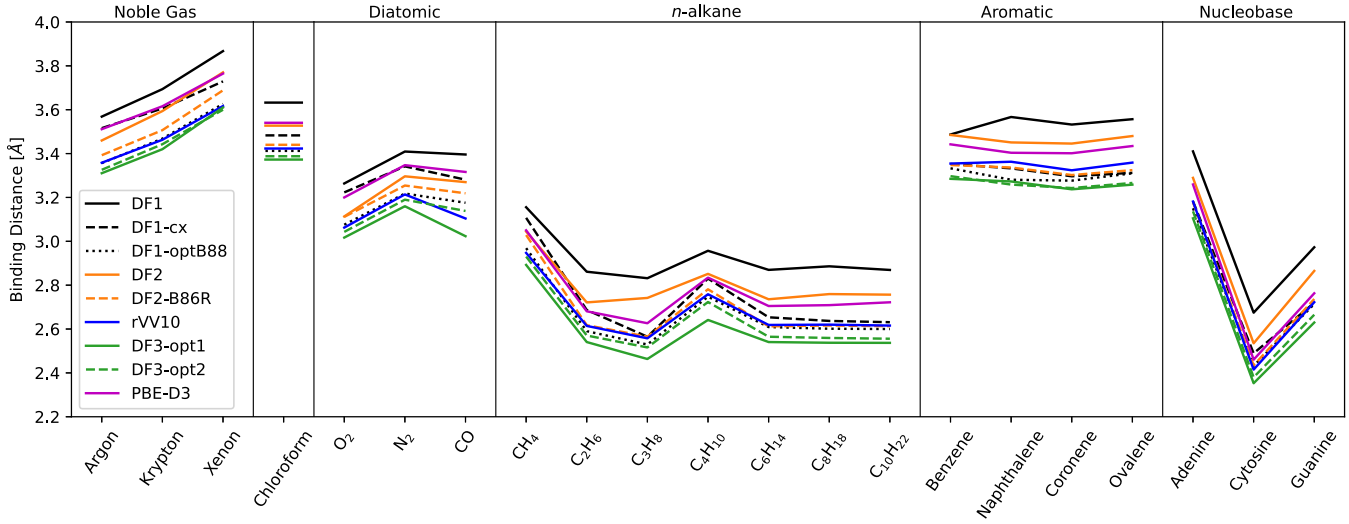

FIG. 3. Binding distances for all systems in the benchmark set. Vertical lines divide each subgroup of the set. All distances are provided in the Supplemental Material [75].

We may also resolve the gradient contribution to the interaction force, defined as

$$\Delta k_{\mathrm{gx}}(s) = -\frac{\mathrm{d}\Delta \mathrm{e}_{\mathrm{gx}}(\mathrm{s})}{\mathrm{d}|a|},$$

where a is the separation between the adsorbate and graphene sheet.

In our illustration of the gradient contribution to the exchange interaction energy $\Delta e_{\mathrm{gx}}(s)$, the DF3-opt1 enhancement factor is used. The overall appearance of the exchange interaction curves has a similar shape for different functionals with a scale factor given by $F(s)/F_{\mathrm{DF3-opt1}}(s)$, in addition to smaller self-consistent effects of updating the electronic density $n(\mathbf{r})$ and the Kohn-Sham orbitals. However, this scaling significantly impacts the binding separations and total energy. To calculate the gradient contribution to the exchange force $\Delta k_{\mathrm{gx}}(s)$ of adsorbed chloroform, we took the difference between two $\Delta e_{\mathrm{gx}}(s)$: one at equilibrium distance from the graphene sheet, and one displaced by 0.1 Å from equilibrium.

In our study, we include several van der Waals density functionals: vdW–DF [27], vdW–DF-optB88 [41], vdW–DF-cx [42], vdW–DF2 [39], vdW–DF2-B86R [43], vdW–DF3-opt1 [44], and vdW–DF3-opt2 [44]. For brevity, they are referred to as DF1, DF1-optB88, DF1-cx, DF2, DF2-B86R, DF3-opt1, and DF3-opt2, respectively. These functionals differ only in their nonlocal correlation and GGA exchange terms. Their enhancement factors $F_{\mathrm{x}}(s)$ are shown in Fig. 2. We also include the nonlocal correlation functionals rVV10 [49]—a revision of the earlier VV10 [48] that is better suited for plane waves—and the popular force-field dispersion-corrected GGA [76] variant PBE-D3 [33], with zero-damping. While these cannot be compared with the van der Waals density functionals through a reduced-gradient analysis focused solely on the exchange, we nonetheless include them in the benchmark study.

III. RESULTS AND ANALYSIS

A. Lattice constants

The full results of our benchmark for the graphene lattice constants are given in the Supplemental Material [75]. All the functionals predict experimental lattice constants with an absolute relative deviation less than 1%. Among them, vdW–DF1-cx and vdW–DF3-opt1 have the best agreement with experiment, both falling within the range of the reported measurement error [77].

B. Adsorption distances

Figure 3 shows the distance between each of our adsorbates and the graphene substrate for all of the tested functionals. DF1 demonstrates the greatest adsorption distance for every adsorbate studied. This can be traced back to its exchange form, as neither DF1-cx nor DF1-optB88 follow the same trends. The difference in separations for DF2 and DF2-B86R is smaller, with notable exceptions for the aromatic hydrocarbons and certain n-alkanes. In these cases, separations predicted by DF2 exceed those of DF2-B86R by as much as 0.1 Å. DF3-opt1 and DF3-opt2 also deviate little from one another.

Figure 4 shows $\Delta k_{\mathrm{gx}}(s)$ for adsorbed chloroform. This force is relevant to the binding distance and is generally dependent on lower values of s than the energy. Comparing this curve with each functional's enhancement factor in Fig. 2 can explain much of the trend; in particular, the position of the zero crossing, here around $s = 1.2$, is crucial. For DF1, we see that the positive region of $\Delta k_{\mathrm{gx}}(s)$ beyond that point is enhanced much more than the negative region, resulting in a greater repulsive contribution from the gradient exchange. DF2 predicts similarly large binding distances and had previously been observed to overestimate solid lattice constants due to the fact that its PW86r enhancement factor grows very quickly in the region of $s < 0.5$. DF2-B86R implements an enhancement factor that increases slower in the low-s limit,

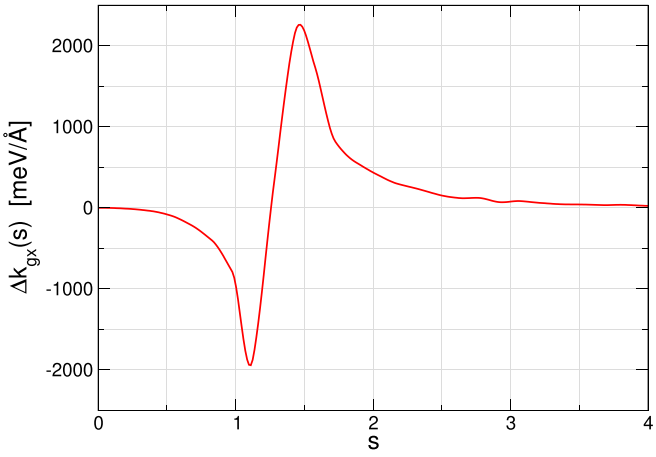

FIG. 4. s-resolved gradient contribution to the exchange interaction force $\Delta k_{gx}(s)$ between chloroform and graphene.

as can be seen by its derivative in Fig. 2. This reduced enhancement is also present in higher ranges of s, which are more relevant to dispersion-based geometries. For this reason, DF2-B86R displays shorter binding distances than DF2 within our study.

C. Adsorption energies

Figure 5 shows the adsorption energies and respective relative deviations for all systems in our dataset. The accuracy varies significantly between the different functionals, with variants using DF1 correlation tending to overestimate binding energies while PBE-D3 and the later DF2 variants slightly underestimate on average. DF2 takes a coefficient of the internal exchange, $Z_{ab} = -1.887$, that is larger than that of DF1, -0.8491, effectively "scaling" the dispersion interactions to larger separations and causing reduced dispersion interactions [20,51]. This corrects for the overbinding in the molecular dimers [39,78], and has also resulted in smaller binding for other classes of systems [44].

rVV10 and the two DF3 variants generally give relative deviations between those of DF1 and DF2 variants. While the optimizations of DF3 take different Z_{ab}, DF3-opt1 being that of DF1 and DF3-opt2 being that of DF2, they also use a form of the nonlocal correlation that is based on a

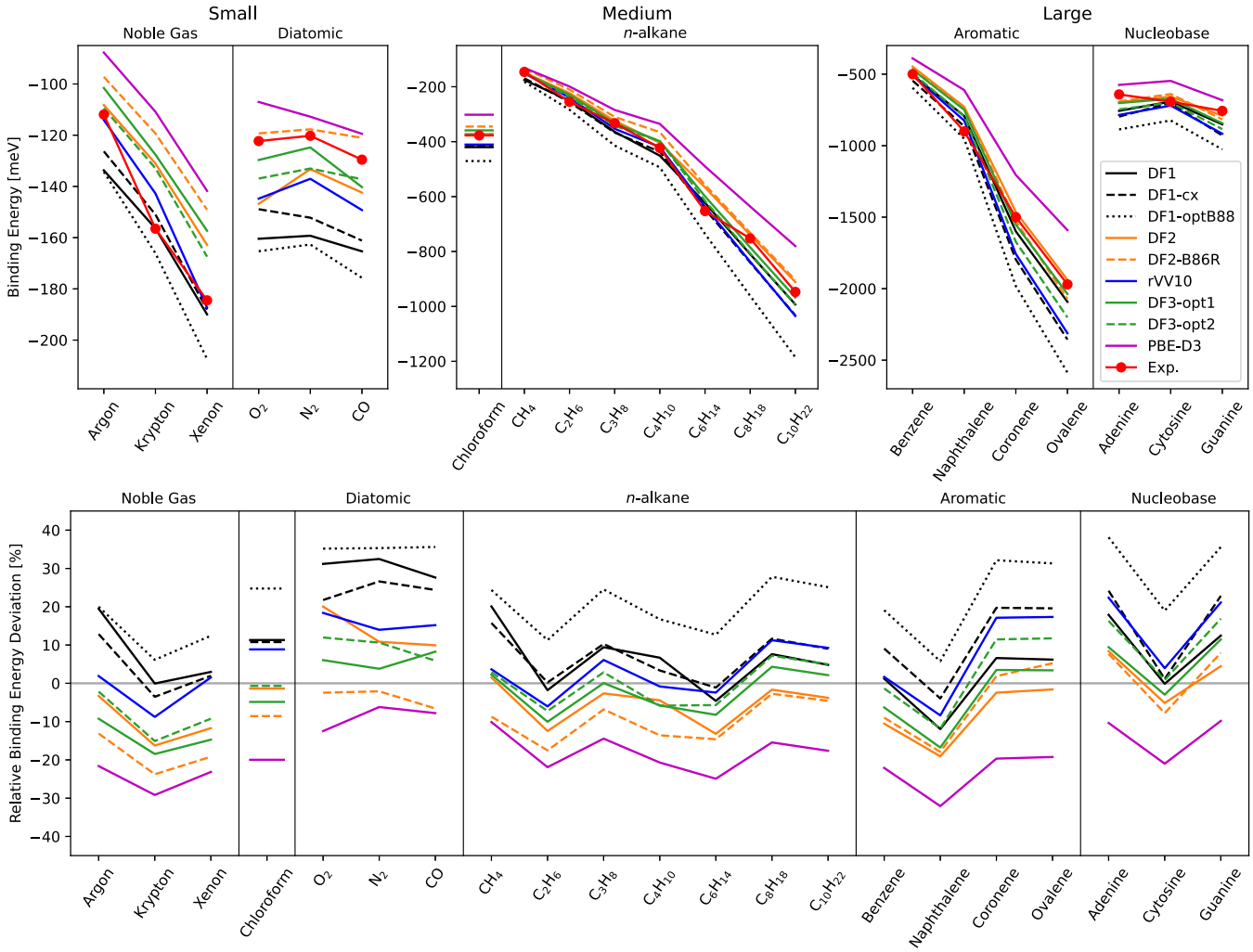

FIG. 5. Interaction energies (top) and relative deviations in the interaction energy (bottom) for all systems in the benchmark set. All energies and deviations are provided in the Supplemental Material [75].

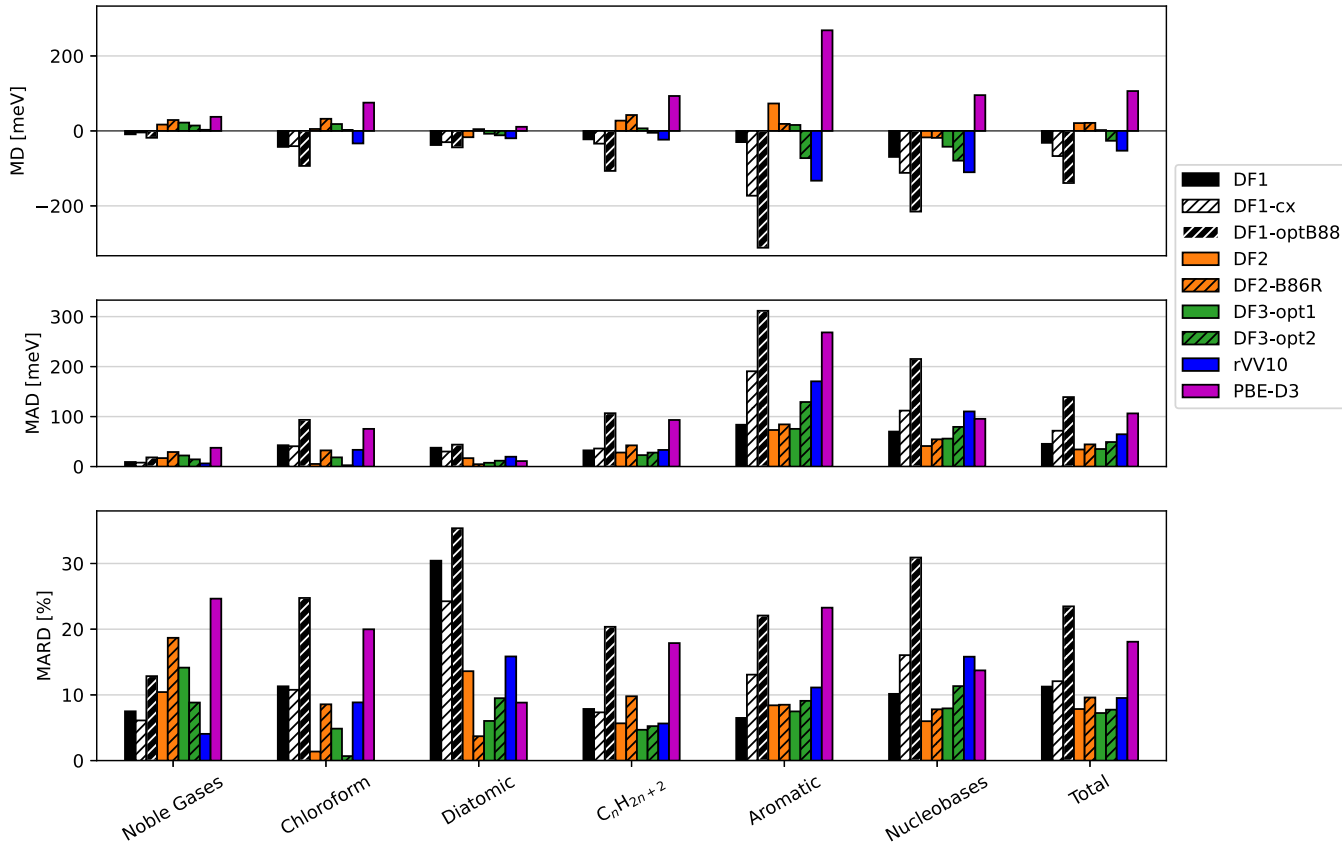

FIG. 6. Comparison of mean deviation (MD), mean absolute deviation (MAD), and mean absolute relative deviation (MARD) for six classes of graphene adsorption systems. Individual system energies, as well as the MD, MAD, and MARD of each class, are provided in the Supplemental Material [75].

different dispersion model than the previous generations. These new vdW-DF3 functionals also improved performance for a broad variety of systems, including benzene-to-metal surface adsorption, which is structurally similar to the systems in our benchmark.

It is notable that the noble gases, diatomic molecules, and nucleobases all deviate from the observed trends of DF1-, DF2-, and DF3-type functionals. More functionals tend to underestimate the binding of noble gases and overestimate that of the diatomic molecules. The binding of adenine and guanine are also more often overestimated, although this trend does not extend to cytosine.

Figure 6 shows the mean deviations (MD), mean absolute deviations (MAD), and mean absolute relative deviations (MARD) of all system classes in our dataset. Due to the weak-binding nature of the diatomics and nucleobases, the MARD's of DF1 generation functionals are all high for those systems, exceeding 10% in all cases. For other system classes, the *n*-alkanes and aromatic hydrocarbons, accuracy is dependent on size. As Fig. 5 shows, relative deviations in binding energy tend to increase slightly with respect to *n*-alkane size. For aromatics, the experimental binding energies shift from strong to weak binding as adsorbates increase in size, particularly between naphthalene and coronene.

In Fig. 7 we show two components of the adsorption energy for each of the *n*-alkanes in our study, the nonlocal correlation and gradient contribution to exchange, adjusted

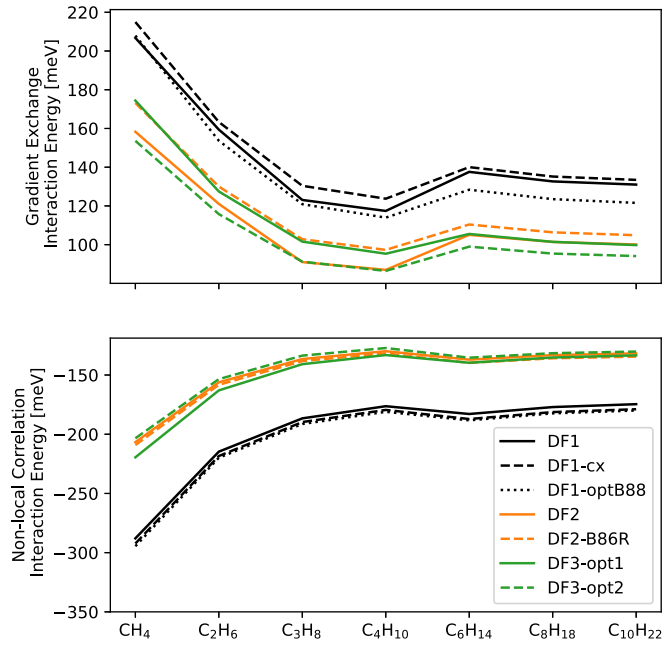

FIG. 7. Components of the adsorption energy of the *n*-alkanes (per carbon atom) on graphene, as calculated by each of the van der Waals density functionals in our study.

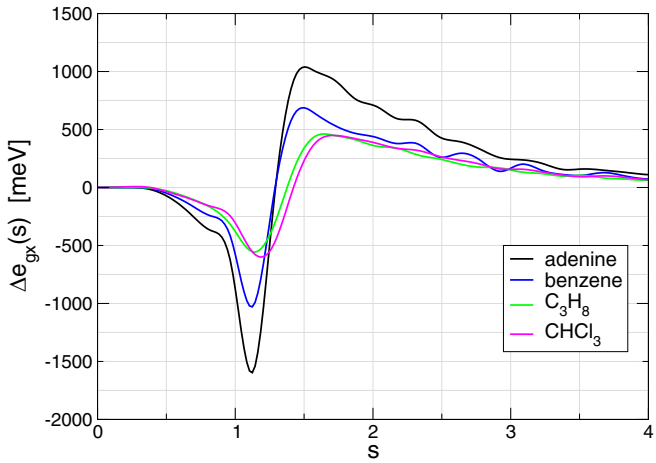

FIG. 8. s-resolved gradient exchange interaction energy $\Delta e_{\mathrm{gx}}(s)$ for some representative systems within our study: adenine from the nucleobases, benzene from the aromatic hydrocarbons, propane from the n-alkanes, and chloroform.

for the number of carbon atoms in each molecule. With the nonlocal correlation providing an attractive contribution and the gradient exchange providing a repulsive contribution, the overbinding of DF1-type functionals can be traced to the large nonlocal correlation that is not sufficiently compensated by the gradient exchange form. We also note that the nonlocal contributions of DF2 and DF3 are very similar for this class of systems. This benefits the accuracy of DF3-opt1 in particular, which has a slightly smaller gradient exchange contribution that prevents it from underbinding to the same extent as DF2 and DF2-B86R.

D. Reduced-gradient analysis of binding energies

To further understand the factors that drive functional performance in our study, we make use of reduced-gradient analysis. As outlined in the Introduction, we begin with the generalized gradient approximation of exchange and isolate contributions from the gradient of the charge density. For a given system, we resolve the gradient contribution to the interaction energy as a function of the reduced density gradient s, a dimensionless parameter that forms the argument of the exchange enhancement factor $F_{\mathrm{x}}(s)$. This s-resolved gradient contribution to the exchange interaction is denoted by $\Delta e_{\mathrm{gx}}(s)$. By calculating $\Delta e_{\mathrm{gx}}(s)$ for select systems in our dataset, we reveal which values of the reduced gradient contribute the most to interaction energy. This, in turn, allows us to draw a line of cause-and-effect between the shape of a van der Waals density functional's exchange enhancement factor and its performance.

Figure 8 shows $\Delta e_{\mathrm{gx}}(s)$ curves for a few representative systems in our benchmark. Each curve possesses a negative region, causing attraction, and a positive region, causing repulsion. The mechanism by which the gradient exchange transitions from attraction to repulsion can be elegantly described in terms of the topological evolution of s isosurfaces, which is discussed in the Appendix. For our analysis, we use the ratio $F_{\mathrm{x}}(s_{\mathrm{max}})/F_{\mathrm{x}}(s_{\mathrm{min}})$ as a shorthand for how a given enhancement factor balances these two regions, with s_{min} and s_{max} denoting the location of peaks in the negative and positive region, respectively. The larger this ratio is for a given functional, the more repulsive is its gradient contribution to the exchange interaction energy.

We can demonstrate this with the example of adsorbed chloroform, which has a s_{min} and s_{max} of 1.19 and 1.71, respectively. DF1-optB88 severely overbinds this system to a degree that ordinary DF1 and DF1-cx do not. We trace this behavior directly to their respective enhancement factors, as the ratio $F_{\mathrm{x}}(s_{\mathrm{max}})/F_{\mathrm{x}}(s_{\mathrm{min}})$ is 1.142, 1.129, and 1.117 for DF1, DF1-cx, and DF1-optB88, respectively. As a result, DF1-optB88 receives a smaller repulsive contribution from exchange, insufficient to offset the strong binding of DF1's nonlocal correlation.

We also apply our analysis to the entire benchmark set in aggregate. For the $\Delta e_{\mathrm{gx}}(s)$ curves in Fig. 8 we find an average s_{min} of 1.18 and an average s_{max} of 1.79. The corresponding $F_{\mathrm{x}}(s_{\mathrm{max}})/F_{\mathrm{x}}(s_{\mathrm{min}})$ ratios are 1.167 for DF1, 1.154 for DF1-cx, and 1.138 for DF1-optB88, so we expect the average exchange energies to scale as DF1 > cx13 > optB88. This is exactly what we see in Fig. 6, with MDs of −32, −67, and −140 meV for DF1, DF1-cx, and DF1-optB88, respectively. All three overestimate binding however, which suggests that a functional with DF1 nonlocal correlation should have an enhancement factor that increases more sharply in the regime of $1.18 < s < 1.79$ in order to describe these systems accurately.

We draw a similar comparison between DF2 and DF2-B86R, as they are both identical to one another except for their forms of the enhancement factor. The ratio $F_{\mathrm{x}}(1.79)/F_{\mathrm{x}}(1.18)$ is 1.127 for ordinary DF2 and 1.124 for DF2-B86R, although the B86R enhancement factor increases more quickly beyond $s = 1.8$, suggesting that the interaction energy of these two functionals should be nearly the same across our entire set, but that DF2-B86R's should be slightly larger. Again this is exactly what we observe, with DF2 having an overall MD of 20.9 meV, just a bit lower than DF2-B86R's 21.4 meV. The underestimation of binding energies by these two functionals suggests the need for a slowly increasing enhancement factor in the regime of $1.2 < s < 1.8$. This is in fact fulfilled by DF3-opt2 in its revised B86b form. While DF3-opt2's nonlocal correlation differs from that DF2, the second optimization was designed to be an improved analog to DF2 in both its exchange and correlation. Indicative of this, DF3-opt2 has $F_{\mathrm{x}}(1.79)/F_{\mathrm{x}}(1.18) = 1.106$, significantly smaller than either of the DF2 forms.

A motivation for analyzing the set in aggregate is to compare the s signature with other types of systems. In Ref. [68], we calculated the s signatures of molecular dimers in the S22 test set, molecular crystals in the X23 test set, several layered systems, and three coinage metals with adsorbed benzene. These signatures are characterized in part by the s value at which gradient exchange contributions switch from negative to positive, called $s_0^{\Delta e}$. For the graphene adsorption systems analyzed here, we find an average $s_0^{\Delta e}$ of 1.41. Of the systems studied in Ref. [68], by far the closest to this are the X23 molecular crystals with an average $s_0^{\Delta e}$ of 1.44, followed by dispersion-bonded dimers at 1.51. The other system types—hydrogen-bonded dimers, layered systems, and benzene-metal adsorption systems—all averaged less than 1.2 in $s_0^{\Delta e}$. For future functional development, this

would suggest a low degree of tunability between graphene adsorption and molecular crystals. The good performance of DF3 for graphene adsorption, and its subpar performance in the X23 [44], illustrates the challenges of further improving the accuracy within the vdW-DF framework. However, the *s* signatures of our graphene dataset are much more diverse than those of the X23 or S22, which makes it a valuable benchmark set for functionals.

IV. CONCLUSION

We have presented a benchmark study of the adsorption of molecules onto graphene, and in the process we have compared the accuracy of various van der Waals density functionals from each of the first three generations. We have found that all functionals perform well in the calculation of the graphene lattice constant, but that significant differences lie in the adsorption energies. vdW–DF2 and the two forms of vdW–DF3, opt1 and opt2, show the best accuracy out of the functionals tested. We find that the first generation of vdW–DF broadly overestimates binding energies, and that this effect is mitigated or exacerbated by the choice in the GGA exchange, as shown by the difference between DF1 and DF1-optB88. The nonlocal correlation functional rVV10 also shows good accuracy within our set. However, its performance is also unbalanced; it excels in modeling noble gas and *n*-alkane adsorption but falls behind in the case of nucleobases and diatomic molecules. Despite good accuracy in our benchmark, it is worth keeping in mind that DF2 struggles more broadly with coinage metal surface adsorption, interlayer separations (including that of graphite), and solid lattice constants [43,44,79–81]. We also find that PBE-D3 almost always underestimates binding by a significant amount.

We have also shown how reduced-gradient analysis can be used to account for the differences between different variants of vdW–DF within each vdW–DF generation. This analysis shows that *s* values of 1.18 and 1.79 are the most significant contributors to the adsorption energy of these systems, and that the accuracy of a functional for a given nonlocal correlation is largely dependent on the shape of its exchange enhancement factor between these two points. Our analysis also provides insight as to what characteristics help or hurt a functional's evaluation of a given system, revealing matches of the GGA exchange to each nonlocal correlation that optimize the accuracy of the interaction energy.

In summary, we find that the most recent vdW–DF generation, vdW–DF3, offers not just improved accuracy but improved consistency over past functionals that have sought to model long-range dispersion interactions. Moreover, the insights provided by reduced-gradient analysis point to avenues

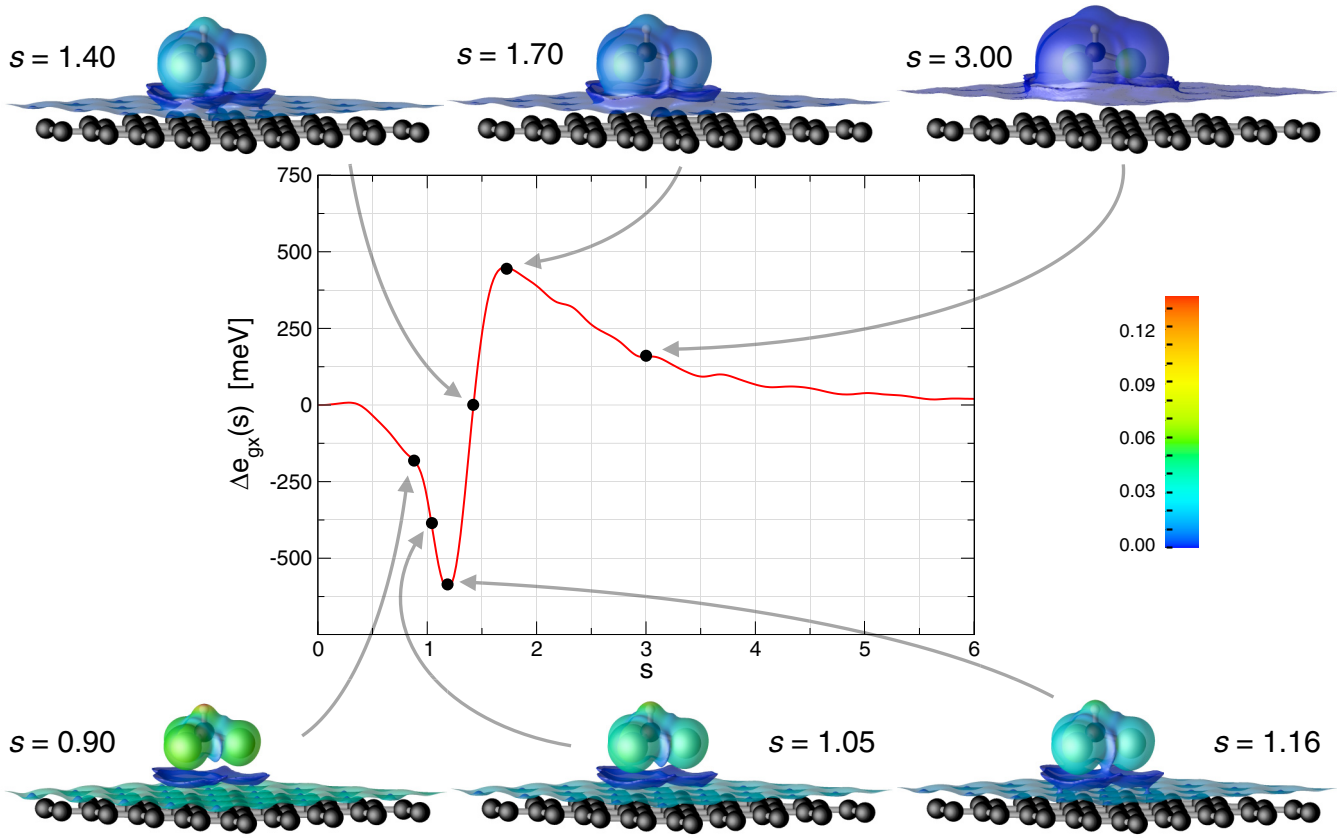

FIG. 9. Isosurfaces of *s* in $CHCl_3$ adsorbed onto graphene with their corresponding values of $\Delta e_{gx}(s)$, as generated using vdW–DF3-opt1. Charge density [e/Bohr^3] is color mapped onto each isosurface. Although plots of charge transfer during bond formation [82–86] show some similarities to isosurfaces of *s*, they convey an important but fundamentally different concept of van der Waals bonding that is less relevant in the context of a reduced-gradient analysis.

of improvement for several of the functionals in our study. These insights can guide further functional development for dispersion-bonded systems.

ACKNOWLEDGMENTS

This work was supported by the U.S. National Science Foundation Grant No. DMR–1712425. The computations in this work were done on the high-performance cluster Saga and Fram managed by UNINETT Sigma2. Work in Norway was supported in part by the Research Council of Norway in the FOX project (Project No. 302362).

APPENDIX: REDUCED-GRADIENT ANALYSIS

Reference [68] describes the mechanism by which gradient exchange contributions switch from attractive to repulsive with increasing s. For a broad array of systems including molecular dimers, molecular crystals, and layered structures, this process is shown to be the result of a topological change between the s isosurfaces of a given system. Figure 9 shows several isosurfaces of s for graphene-adsorbed chloroform. Each isosurface of s corresponds to a point in chloroform's $\Delta e_{\rm gx}(s)$ that contributes to the exchange energy. Onto each isosurface we map the charge density as a color. When calculating the exchange energy of a certain s value, we are effectively integrating over the two-dimensional space of the isosurface according to Eq. (2), so areas of high charge density contribute more to the energy. For $s = 0.90$ there are three distinct surfaces of s: one around the chloroform molecule, one above the graphene substrate, and one in between them. When calculating the interaction energy of this system using Eq. (3), we subtract out the chloroform and substrate surfaces, leaving only the "disk" in the center. The charge density on this disk forms the sole negative contribution to $\Delta e_{\rm gx}(s = 0.90)$. When we increase the iso-value to $s = 1.05$, each of the three surfaces grow outward from their respective center points. Now not only is the disk larger, giving more area to integrate over for the exchange, but the charge density on the surface is higher due to its closer proximity to the molecule and substrate. As a result there is an increase in the negative exchange interaction, which is reflected by a downward slope in $\Delta e_{\rm gx}(s = 1.05)$. At $s = 1.16$ the central disk begins to merge with the molecule and substrate surfaces, meaning that positive contributions from $e_{\rm gx}^{\rm system}$ in Eq. (3) are no longer being canceled out. As a direct consequence, $\Delta e_{\rm gx}(s)$ shifts to a positive energy. Then, at larger isovalues such as $s = 1.40$, 1.70, and 3.00, the merger completes itself and $\Delta e_{\rm gx}(s)$ regresses asymptotically to zero due to a lowering of charge density as the s isosurface grows farther away from the molecules.

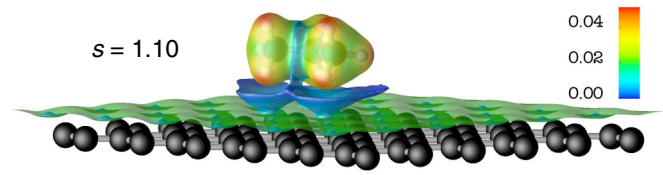

FIG. 10. An isosurface of $s = 1.10$ in a butane-graphene complex with charge density [e/Bohr^3] in color mapped onto the surface. Charge densities were obtained using the DF3-opt1 functional.

This pattern of expansion, merging, and regression that dictates the rise and fall of the gradient exchange interaction can also be seen in all other systems. We show this using the butane-graphene complex as an example, shown in Fig. 10. Even though butane is highly dissimilar from chloroform in its geometry, we still see the same three isosurfaces: one surrounding the butane molecule, one above the graphene sheet, and an interactive "disk" in the middle. Note that at an isosurface of $s = 1.10$ as shown in the figure, the disk has barely begun to merge with the other surfaces at its edges. Accordingly, butane's $\Delta e_{\rm gx}(s)$ curve in Fig. 8 reaches a global minimum at around this point and then begins to increase with higher s.

[1] Y. Tang, Z. Yang, and X. Dai, A theoretical simulation on the catalytic oxidation of Co on Pt/graphene, Phys. Chem. Chem. Phys. **14**, 16566 (2012).

[2] M. Groves, A. Chan, C. Malardier-Jugroot, and M. Jugroot, Improving platinum catalyst binding energy to graphene through nitrogen doping, Chem. Phys. Lett. **481**, 214 (2009).

[3] K. Takeuchi, S. Yamamoto, Y. Hamamoto, Y. Shiozawa, K. Tashima, H. Fukidome, T. Koitaya, K. Mukai, S. Yoshimoto, M. Suemitsu, Y. Morikawa, J. Yoshinobu, and I. Matsuda, Adsorption of CO_2 on graphene: A combined TPD, XPS, and vdw-DF study, J. Phys. Chem. C **121**, 2807 (2017).

[4] J. Ma, A. Michaelides, D. Alfè, L. Schimka, G. Kresse, and E. Wang, Adsorption and diffusion of water on graphene from first principles, Phys. Rev. B **84**, 033402 (2011).

[5] I. Hamada, Adsorption of water on graphene: A van der Waals density functional study, Phys. Rev. B **86**, 195436 (2012).

[6] K. R. Paserba and A. J. Gellman, Effects of conformational isomerism on the desorption kinetics of n-alkanes from graphite, J. Chem. Phys. **115**, 6737 (2001).

[7] R. Zhang, X. Yu, Q. Yang, G. Cui, and Z. Li, The role of graphene in anti-corrosion coatings: A review, Constr. Build. Mater. **294**, 123613 (2021).

[8] D. J. Burke and W. A. Brown, Ice in space: Surface science investigations of the thermal desorption of model interstellar ices on dust grain analogue surfaces, Phys. Chem. Chem. Phys. **12**, 5947 (2010).

[9] F. Schedin, A. K. Geim, S. V. Morozov, E. W. Hill, P. Blake, M. I. Katsnelson, and K. S. Novoselov, Detection of individual gas molecules adsorbed on graphene, Nat. Mater. **6**, 652 (2007).

[10] Y. Dan, Y. Lu, N. J. Kybert, Z. Luo, and A. T. C. Johnson, Intrinsic response of graphene vapor sensors, Nano Lett. **9**, 1472 (2009).

[11] A. Paton-Carrero, P. Sanchez, L. Sánchez-Silva, and A. Romero, Graphene-based materials behaviour for dyes adsorption, Mater. Today Commun. **30**, 103033 (2022).

[12] M. Sweetman, S. May, N. Mebberson, P. Pendleton, K. Vasilev, S. Plush, and J. Hayball, Activated carbon, carbon nanotubes and graphene: Materials and composites for advanced water purification, J. Carbon Res. **3**, 18 (2017).

[13] Y. Xu, H. Bai, G. Lu, C. Li, and G. Shi, Flexible graphene films via the filtration of water-soluble noncovalent functionalized graphene sheets, J. Am. Chem. Soc. **130**, 5856 (2008).

[14] Y. Han, Z. Xu, and C. Gao, Ultrathin graphene nanofiltration membrane for water purification, Adv. Funct. Mater. **23**, 3693 (2013).

[15] A. Aghigh, V. Alizadeh, H. Wong, M. S. Islam, N. Amin, and M. Zaman, Recent advances in utilization of graphene for filtration and desalination of water: A review, Desalination **365**, 389 (2015).

[16] D. B. Wells, M. Belkin, J. Comer, and A. Aksimentiev, Assessing graphene nanopores for sequencing DNA, Nano Lett. **12**, 4117 (2012).

[17] S. J. Heerema and C. Dekker, Graphene nanodevices for DNA sequencing, Nat. Nanotechnol. **11**, 127 (2016).

[18] H. W. C. Postma, Rapid sequencing of individual DNA molecules in graphene nanogaps, Nano Lett. **10**, 420 (2010).

[19] Z. Wang, S. Wu, L. Colombi Ciacchi, and G. Wei, Graphene-based nanoplatforms for surface-enhanced Raman scattering sensing, Analyst **143**, 5074 (2018).

[20] K. Berland, V. R. Cooper, K. Lee, E. Schröder, T. Thonhauser, P. Hyldgaard, and B. I. Lundqvist, Van der Waals forces in density functional theory: A review of the vdW-DF method, Rep. Prog. Phys. **78**, 066501 (2015).

[21] S. Grimme, Density functional theory with london dispersion corrections, Wiley Interdiscip. Rev. Comput. Mol. Sci. **1**, 211 (2011).

[22] K. Burke, Perspective on density functional theory, J. Chem. Phys. **136**, 150901 (2012).

[23] J. Klimeš and A. Michaelides, Perspective: Advances and challenges in treating van der Waals dispersion forces in density functional theory, J. Chem. Phys. **137**, 120901 (2012).

[24] S. F. Sousa, P. A. Fernandes, and M. J. Ramos, General performance of density functionals, J. Phys. Chem. A **111**, 10439 (2007).

[25] A. Pribram-Jones, D. A. Gross, and K. Burke, DFT: A theory full of holes? Annu. Rev. Phys. Chem. **66**, 283 (2015).

[26] S. Grimme, Accurate description of van der Waals complexes by density functional theory including empirical corrections, J. Comput. Chem. **25**, 1463 (2004).

[27] M. Dion, H. Rydberg, E. Schröder, D. C. Langreth, and B. I. Lundqvist, Van der Waals density functional for general geometries, Phys. Rev. Lett. **92**, 246401 (2004).

[28] S. Tsuzuki, H. Houjou, Y. Nagawa, M. Goto, and K. Hiratani, Cooperative enhancement of water binding to crownophane by multiple hydrogen bonds: Analysis by high level *ab initio* calculations, J. Am. Chem. Soc. **123**, 4255 (2001).

[29] U. Zimmerli, M. Parrinello, and P. Koumoutsakos, Dispersion corrections to density functionals for water aromatic interactions, J. Chem. Phys. **120**, 2693 (2004).

[30] M. J. Allen and D. J. Tozer, Helium dimer dispersion forces and correlation potentials in density functional theory, J. Chem. Phys. **117**, 11113 (2002).

[31] A. Tkatchenko and O. A. von Lilienfeld, Adsorption of Ar on graphite using london dispersion forces corrected Kohn-Sham density functional theory, Phys. Rev. B **73**, 153406 (2006).

[32] S. Grimme, Semiempirical GGA-type density functional constructed with a long-range dispersion correction, J. Comput. Chem. **27**, 1787 (2006).

[33] S. Grimme, J. Antony, S. Ehrlich, and H. Krieg, A consistent and accurate *ab initio* parametrization of density functional dispersion correction (DFT-D) for the 94 elements H-Pu, J. Chem. Phys. **132**, 154104 (2010).

[34] E. Caldeweyher, S. Ehlert, A. Hansen, H. Neugebauer, S. Spicher, C. Bannwarth, and S. Grimme, A generally applicable atomic-charge dependent london dispersion correction, J. Chem. Phys. **150**, 154122 (2019).

[35] J. Tao, J. P. Perdew, V. N. Staroverov, and G. E. Scuseria, Climbing the density functional ladder: Nonempirical meta-generalized gradient approximation designed for molecules and solids, Phys. Rev. Lett. **91**, 146401 (2003).

[36] Y. Zhao and D. G. Truhlar, A new local density functional for main-group thermochemistry, transition metal bonding, thermochemical kinetics, and noncovalent interactions, J. Chem. Phys. **125**, 194101 (2006).

[37] J. Sun, A. Ruzsinszky, and J. P. Perdew, Strongly constrained and appropriately normed semilocal density functional, Phys. Rev. Lett. **115**, 036402 (2015).

[38] J. W. Furness, A. D. Kaplan, J. Ning, J. P. Perdew, and J. Sun, Accurate and numerically efficient r^2 SCAN meta-generalized gradient approximation, J. Phys. Chem. Lett. **11**, 8208 (2020).

[39] K. Lee, É. D. Murray, L. Kong, B. I. Lundqvist, and D. C. Langreth, Higher-accuracy van der Waals density functional, Phys. Rev. B **82**, 081101(R) (2010).

[40] V. R. Cooper, Van der Waals density functional: An appropriate exchange functional, Phys. Rev. B **81**, 161104(R) (2010).

[41] J. Klimeš, D. R. Bowler, and A. Michaelides, Chemical accuracy for the van der Waals density functional, J. Phys.: Condens. Matter **22**, 022201 (2010).

[42] K. Berland and P. Hyldgaard, Exchange functional that tests the robustness of the plasmon description of the van der Waals density functional, Phys. Rev. B **89**, 035412 (2014).

[43] I. Hamada, van der Waals density functional made accurate, Phys. Rev. B **89**, 121103(R) (2014).

[44] D. Chakraborty, K. Berland, and T. Thonhauser, Next-generation nonlocal van der Waals density functional, J. Chem. Theory Comput. **16**, 5893 (2020).

[45] K. Berland, D. Chakraborty, and T. Thonhauser, van der Waals density functional with corrected C_6 coefficients, Phys. Rev. B **99**, 195418 (2019).

[46] K. Berland, Y. Jiao, J.-H. Lee, T. Rangel, J. B. Neaton, and P. Hyldgaard, Assessment of two hybrid van der Waals density functionals for covalent and non-covalent binding of molecules, J. Chem. Phys. **146**, 234106 (2017).

[47] V. Shukla, Y. Jiao, J. H. Lee, E. Schröder, J. B. Neaton, and P. Hyldgaard, Accurate nonempirical range-separated hybrid van der Waals density functional for complex molecular problems, solids, and surfaces, Phys. Rev. X **12**, 041003 (2022).

[48] O. A. Vydrov and T. Van Voorhis, Nonlocal van der Waals density functional: The simpler the better, J. Chem. Phys. **133**, 244103 (2010).

[49] R. Sabatini, T. Gorni, and S. de Gironcoli, Nonlocal van der Waals density functional made simple and efficient, Phys. Rev. B **87**, 041108(R) (2013).
[50] É. D. Murray, K. Lee, and D. C. Langreth, Investigation of exchange energy density functional accuracy for interacting molecules, J. Chem. Theory Comput. **5**, 2754 (2009).
[51] K. Berland and P. Hyldgaard, Analysis of van der Waals density functional components: Binding and corrugation of benzene and C_{60} on boron nitride and graphene, Phys. Rev. B **87**, 205421 (2013).
[52] S. D. Chakarova-Käck, E. Schröder, B. I. Lundqvist, and D. C. Langreth, Application of van der Waals density functional to an extended system: Adsorption of benzene and naphthalene on graphite, Phys. Rev. Lett. **96**, 146107 (2006).
[53] Ø. Borck and E. Schröder, Methylbenzenes on graphene, Surf. Sci. **664**, 162 (2017).
[54] E. Schröder, Methanol adsorption on graphene, J. Nanomater. **2013**, 1 (2013).
[55] E. Londero, E. K. Karlson, M. Landahl, D. Ostrovskii, J. D. Rydberg, and E. Schröder, Desorption of n-alkanes from graphene: A van der Waals density functional study, J. Phys.: Condens. Matter **24**, 424212 (2012).
[56] D. Le, A. Kara, E. Schröder, P. Hyldgaard, and T. S. Rahman, Physisorption of nucleobases on graphene: A comparative van der Waals study, J. Phys.: Condens. Matter **24**, 424210 (2012).
[57] J. Åkesson, O. Sundborg, O. Wahlström, and E. Schröder, A van der Waals density functional study of chloroform and other trihalomethanes on graphene, J. Chem. Phys. **137**, 174702 (2012).
[58] K. Berland, S. D. Chakarova-Käck, V. R. Cooper, D. C. Langreth, and E. Schröder, A van der Waals density functional study of adenine on graphene: Single-molecular adsorption and overlayer binding, J. Phys.: Condens. Matter **23**, 135001 (2011).
[59] S. D. Chakarova-Käck, Ø. Borck, E. Schröder, and B. I. Lundqvist, Adsorption of phenol on graphite(0001) and α-Al_2O_3(0001): Nature of van der Waals bonds from first-principles calculations, Phys. Rev. B **74**, 155402 (2006).
[60] R. S. Smith, R. A. May, and B. D. Kay, Desorption kinetics of Ar, Kr, Xe, N_2, O_2, CO, methane, ethane, and propane from graphene and amorphous solid water surfaces, J. Phys. Chem. B **120**, 1979 (2016).
[61] T. R. Rybolt, D. L. Logan, M. W. Millburn, H. E. Thomas, and A. B. Waters, Correlations of Henry's law gas-solid virial coefficients and chromatographic retention times for hydrocarbons and halocarbons adsorbed on carbopack C carbon, J. Colloid Interface Sci. **220**, 148 (1999).
[62] S. L. Tait, Z. Dohnálek, C. T. Campbell, and B. D. Kay, n-alkanes on Pt(111) and on C(0001)/Pt(111): Chain length dependence of kinetic desorption parameters, J. Chem. Phys. **125**, 234308 (2006).
[63] R. Zacharia, H. Ulbricht, and T. Hertel, Interlayer cohesive energy of graphite from thermal desorption of polyaromatic hydrocarbons, Phys. Rev. B **69**, 155406 (2004).
[64] N. Varghese, U. Mogera, A. Govindaraj, A. Das, P. K. Maiti, A. K. Sood, and C. N. R. Rao, Binding of DNA nucleobases and nucleosides with graphene, ChemPhysChem **10**, 206 (2009).
[65] P. A. Redhead, Thermal desorption of gases, Vacuum **12**, 203 (1962).
[66] E. Freire, O. L. Mayorga, and M. Straume, Isothermal titration calorimetry, Anal. Chem. **62**, 950A (1990).
[67] S. Greene and H. Past, The determination of heats of adsorption by gas-solid chromatography, J. Phys. Chem. **62**, 55 (1958).
[68] T. Jenkins, K. Berland, and T. Thonhauser, Reduced-gradient analysis of van der Waals complexes, Electron. Struct. **3**, 034009 (2021).
[69] A. Zupan, J. P. Perdew, K. Burke, and M. Causa, Density-gradient analysis for density functional theory: Application to atoms, Int. J. Quantum Chem. **61**, 835 (1997).
[70] P. Giannozzi, O. Andreussi, T. Brumme, O. Bunau, M. Buongiorno Nardelli, M. Calandra, R. Car, C. Cavazzoni, D. Ceresoli, M. Cococcioni, N. Colonna, I. Carnimeo, A. Dal Corso, S. de Gironcoli, P. Delugas, R. A. DiStasio Jr, A. Ferretti, A. Floris, G. Fratesi, G. Fugallo, R. Gebauer, U. Gerstmann, F. Giustino, T. Gorni, J. Jia, M. Kawamura, H.-Y. Ko, A. Kokalj, E. Kucukbenli, M. Lazzeri, M. Marsili, N. Marzari, F. Mauri, N. L. Nguyen, H.-V. Nguyen, A. Otero-de-la Roza, L. Paulatto, S. Ponce, D. Rocca, R. Sabatini, B. Santra, M. Schlipf, A. P. Seitsonen, A. Smogunov, I. Timrov, T. Thonhauser, P. Umari, N. Vast, X. Wu, and S. Baroni, Advanced capabilities for materials modelling with Quantum ESPRESSO, J. Phys.: Condens. Matter **29**, 465901 (2017).
[71] K. F. Garrity, J. W. Bennett, K. M. Rabe, and D. Vanderbilt, Pseudopotentials for high-throughput DFT calculations, Comput. Mater. Sci. **81**, 446 (2014).
[72] Cortés-Arriagada, Intermolecular driving forces on the adsorption of DNA/RNA nucleobases to graphene and phosphorene: An atomistic perspective from DFT calculations, J. Mol. Liq. **325**, 115229 (2021).
[73] D. Cortés-Arriagada and D. E. Ortega, Effects on the aromatic character of DNA/RNA nucleobases due to its adsorption onto graphene, Int. J. Quantum Chem. **118**, e25699 (2018).
[74] J.-H. Lee, Y.-K. Choi, H.-J. Kim, R. H. Scheicher, and J.-H. Cho, Physisorption of DNA nucleobases on *h*-BN and graphene: vdW-corrected DFT calculations, J. Phys. Chem. C **117**, 13435 (2013).
[75] See Supplemental Material at http://link.aps.org/supplemental/10.1103/PhysRevB.109.035427 for detailed results and a statistical summary of the full dataset.
[76] J. P. Perdew, K. Burke, and M. Ernzerhof, Generalized gradient approximation made simple, Phys. Rev. Lett. **77**, 3865 (1996).
[77] A. H. Castro Neto, F. Guinea, N. M. R. Peres, K. S. Novoselov, and A. K. Geim, The electronic properties of graphene, Rev. Mod. Phys. **81**, 109 (2009).
[78] S. Tsuzuki, T. Kaneko, and K. Sodeyama, Accuracy of intermolecular interaction energies, particularly those of hetero atom containing molecules obtained by van der Waals DFT calculations, ChemistrySelect **8**, e202203754 (2023).
[79] F. Tran, L. Kalantari, B. Traoré, X. Rocquefelte, and P. Blaha, Nonlocal van der Waals functionals for solids: Choosing an appropriate one, Phys. Rev. Mater. **3**, 063602 (2019).
[80] J. Klimeš, D. R. Bowler, and A. Michaelides, Van der Waals density functionals applied to solids, Phys. Rev. B **83**, 195131 (2011).
[81] K. Berland, C. A. Arter, V. R. Cooper, K. Lee, B. I. Lundqvist, E. Schröder, T. Thonhauser, and P. Hyldgaard, van der Waals density functionals built upon the electron-gas tradition: Facing the challenge of competing interactions, J. Chem. Phys. **140**, 18A539 (2014).
[82] H.-Q. Yin, K. Tan, S. Jensen, S. J. Teat, S. Ullah, X. Hei, E. Velasco, K. Oyekan, N. Meyer, X.-Y. Wang, T. Thonhauser,

X.-B. Yin, and J. Li, A switchable sensor and scavenger: Detection and removal of fluorinated chemical species by a luminescent metal-organic framework, Chem. Sci. **12**, 14189 (2021).

[83] K. Tan, S. Ullah, H. Pandey, E. M. Cedeño-Morales, H. Wang, K. Wang, H.-C. Zhou, J. Li, and T. Thonhauser, Competitive adsorption of NH_3 and H_2o in metal-organic framework materials: MOF-74, Chem. Mater. **34**, 7906 (2022).

[84] Y. Lin, L. Yu, S. Ullah, X. Li, H. Wang, Q. Xia, T. Thonhauser, and J. Li, Temperature-programmed separation of hexane isomers by a porous calcium chloranilate metal-organic framework, Angew. Chem., Int. Ed. **61**, e202214060 (2022).

[85] S. Ullah, K. Tan, D. Sensharma, N. Kumar, S. Mukherjee, A. A. Bezrukov, J. Li, M. J. Zaworotko, and T. Thonhauser, CO_2 capture by hybrid ultramicroporous TIFSIX-3-Ni under humid conditions using non-equilibrium cycling, Angew. Chem., Int. Ed. **61**, e202206613 (2022).

[86] E. Velasco, G. Zhang, S. J. Teat, K. Tan, S. Ullah, T. Thonhauser, and J. Li, Luminescent metal-organic framework for the selective detection of aldehydes, Inorg. Chem. (Washington, DC, US) **62**, 16435 (2023).